Band-Tail Recombination in Hybrid Lead Iodide Perovskite

Adam D. Wright, Rebecca L. Milot, Giles E. Eperon, Henry J. Snaith, Michael B. Johnston, and Laura M. Herz*

Traps limit the photovoltaic efficiency and affect the charge transport of optoelectronic devices based on hybrid lead halide perovskites. Understanding the nature and energy scale of these trap states is therefore crucial for the development and optimization of solar cell and laser technology based on these materials. Here, the low-temperature photoluminescence of formamidinium lead triiodide (HC(NH$_2$)$_2$PbI$_3$) is investigated. A power-law time dependence in the emission intensity and an additional low-energy emission peak that exhibits an anomalous relative Stokes shift are observed. Using a rate-equation model and a Monte Carlo simulation, it is revealed that both phenomena arise from an exponential trap-density tail with characteristic energy scale of ≈3 meV. Charge-carrier recombination from sites deep within the tail is found to cause emission with energy downshifted by up to several tens of meV. Hence, such phenomena may in part be responsible for open-circuit voltage losses commonly observed in these materials. In this high-quality hybrid perovskite, trap states thus predominantly comprise a continuum of energetic levels (associated with disorder) rather than discrete trap energy levels (associated, e.g., with elemental vacancies). Hybrid perovskites may therefore be viewed as classic semiconductors whose band-structure picture is moderated by a modest degree of energetic disorder.

1. Introduction

Hybrid lead halide perovskites combine the advantages of facile and inexpensive synthesis via solution processing or vapor deposition techniques,[1] with excellent optoelectronic properties including high charge-carrier mobility, long charge-carrier lifetimes, narrow emission spectra, and high absorption coefficients across the visible spectrum.[2] Hybrid perovskites are most renowned for their successful implementation in solar cells, achieving power conversion efficiencies now exceeding 22%,[3] but perovskite light-emitting diodes[2c,4] and lasers[5] are also attracting intense research attention. In order to operate

A. D. Wright, Dr. R. L. Milot, Dr. G. E. Eperon, Prof. H. J. Snaith,
Prof. M. B. Johnston, Prof. L. M. Herz
Department of Physics
Clarendon Laboratory
University of Oxford
Parks Road, Oxford OX1 3PU, UK
E-mail: laura.herz@physics.ox.ac.uk

efficiently, these devices all require high rates of radiative recombination compared with nonradiative recombination. Therefore, future development will require the understanding and reduction of competing processes,[6] such as the trap-mediated recombination of charge carriers. Sub-bandgap trap states limit the open-circuit voltage in perovskite solar cells,[7] and can act as nonradiative recombination centers, leading to shorter charge-carrier lifetimes[8] and will limit device efficiencies to below the Shockley–Queisser limit.[9] For example, the relatively low open-circuit voltage of Cu$_2$ZnSnS$_4$ (CZTS) solar cells has been attributed to the presence of deep traps.[10]

Despite a wide range of experimental[8,11] and theoretical[10,12] evidence for the presence of trap states in hybrid perovskites, their causes and nature are still largely unknown.[7,13] In particular, it is unclear whether such traps form energetically discrete crystallographic defect levels,[11b,d,14] or instead comprise a distribution of states arising, for example, from structural disorder.[15] Computational simulations have predicted the energies of point defects, and their presence has been inferred from the fluence dependence of photoluminescence (PL) decays.[11d,e] However, the observation of an exponential onset (Urbach tail) in the absorption spectrum of methylammonium lead triiodide perovskite (MAPbI$_3$)[15b,16] is indicative of a disordered system in which the position of the band edges varies spatially or temporally, resulting in potential minima which form a tail of trap states.[17] It has been suggested that the manifestation of traps in hybrid perovskites is influenced by their composition[18] and fabrication method.[19] Thus, knowledge of the physical origin of the traps would aid efforts to reduce their density and depth in order to improve device performance.

In this article, we investigate the distribution of sub-bandgap trap states in formamidinium lead triiodide (FAPbI$_3$), a perovskite material used in some of the most efficient and stable perovskite solar cells.[1b,20] By judicious measurement of the low-temperature PL over six decades of time and intensity, we are able to identify for the first time a power-law intensity decay, which is a known signature of band-tail mediated recombination. This analysis is supported by our observation of a Stokes-shifted emission peak at low temperatures that exhibits an anomalous temperature dependence, in accordance with the temperature-activated movement of charge within a distribution of localized states. We qualitatively reproduce the anomalous relative Stokes shift using both a rate-equation model and a

**ADVANCED
SCIENCE NEWS**
www.advancedsciencenews.com

**ADVANCED
FUNCTIONAL
MATERIALS**
www.afm-journal.de

Monte Carlo simulation, demonstrating the presence of a band tail with characteristic energy ≈3 meV. We further show that this distribution of sub-bandgap states can yield emission several tens of meV below the bandgap energy when it originates from states deep in the tail. We suggest that these band-tail states result from variations in local structure or electrostatic potential caused, for example, by differences in the orientation of the FA cation dipole. Altogether, our results provide new insight into the fundamental cause and nature of trap states in FAPbI$_3$, which we demonstrate to be governed by a continuous energy distribution of trap states that may arise, for example, from structural disorder. As a result, we show that trap states associated with a discrete energetic origin, such as elemental vacancies, substitutions or interstitials, or an indirect energy gap with well-defined single gap energy, cannot be a dominant cause of charge-carrier trapping in FAPbI$_3$.

2. Results

2.1. Time Dependence of PL

To explore the nature of trap states in hybrid lead halide perovskites, we first recorded the time-dependent PL spectra of solution-processed FAPbI$_3$ thin films between 1 ns and 1 ms after excitation and over temperatures from 10 to 100 K. At these low temperatures, the charge carriers have relaxed to the bottom of any trap distribution and nonradiative recombination pathways are suppressed,[5,11a] allowing PL spectra to provide a probe of the full energetic distribution. Transients of the spectrally integrated PL intensity at 10, 20, and 30 K are shown in **Figure 1**a. The transients appear straight on the log–log scale, that is, the decay remarkably follows a power law over six decades of time after excitation. Previously, PL transients from hybrid lead halide perovskites have generally been recorded over much shorter time intervals, over which they are often fitted with monoexponential[21] or biexponential[11b,22] functions, representing one or two monomolecularly decaying charge-carrier ensembles, respectively.[11a] For example, biexponential fits have been applied to PL transients with both an initial fast and subsequent slow component, which have been, respectively, attributed to recombination at defects at the surface and in the bulk of the material.[11b,23] Alternatively, stretched exponentials and functions including the bimolecular band-to-band recombination of charge carriers have been used,[24] as detailed in the Supporting Information. As we show in Figure 1b, all of these functions are unable to describe adequately the power-law PL decay at 10 K over the six decades of time, despite appearing to fit credibly on a semilogarithmic scale over a shorter temporal range (as shown in the inset). Hence, our novel measurement of the PL dynamics for a hybrid perovskite over six decades of time has allowed us to reveal the power-law nature of the charge-carrier recombination dynamics.

Power-law luminescence decays have previously been identified in a wide range of materials other than hybrid perovskites[25] and are indicative of the involvement of localized trap states in charge-carrier recombination.[26] Such decays mathematically arise from the superposition of many exponentially decaying components,[27] which can physically result from the dependence of the depopulation rate of traps on their energetic
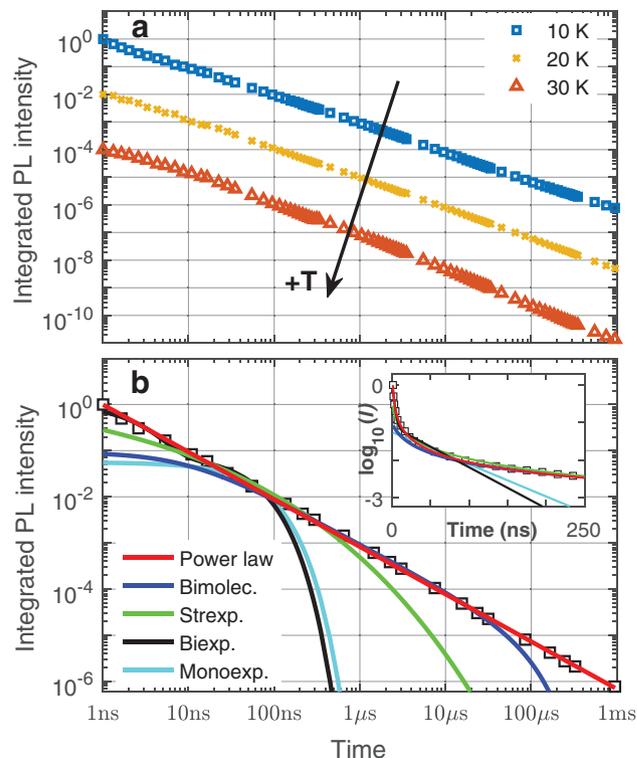
Figure 1. Power-law time dependence of PL intensity. a) Spectrally integrated PL intensity transients of FAPbI$_3$ at 10, 20, and 30 K over six decades of time after excitation, measured for an excitation fluence of 390 nJ cm^{-2}. b) Comparison of power-law fit to PL transient recorded at 10 K with fits of the other functions commonly used to describe PL time decay in hybrid perovskites (combined mono- and bimolecular decay, blue; stretched exponential decay, green; biexponential decay, black; monoexponential decay, cyan). Details of the fits are given in the Supporting Information. The inset shows the difficulty in distinguishing between these fitting functions on a semilogarithmic scale over shorter timescales, where I is the spectrally integrated PL intensity.

depth or spatial separation.[26–28] Whereas a biexponential fit may account for two decay components, a power law expresses the limit when there is a continuous distribution of recombination rates. As detailed in the Supporting Information, models in which the distribution of traps is either exponential in energy or spatially random analytically yield a power-law PL intensity decay to a very good approximation over several decades of time.[27,28] The presence of an energetic distribution of traps is also validated by our observation of a redshift of the PL spectrum with time (Figure S1, Supporting Information), which is consistent with the relaxation and thermalization of charge carriers within a tail of sub-bandgap trap states.[29] Thus, the time dependence of the PL intensity and spectra at 10 K suggests that the traps in these materials form a band tail, rather than energetically discrete levels. Such band tails have been shown to be a common feature in a wide range of other semiconductors,[30] where they result from structural disorder due to defects, doping, or non-uniformity of composition. This disorder causes local potential minima in the conduction or valence bands, which form a density of band-tail states[15a] that is typically modeled as either Gaussian or exponential.[31] The observation of Urbach tails[15,16b] in the absorption spectrum of MAPbI$_3$ suggests that

ADVANCED
SCIENCE NEWS
www.advancedsciencenews.com

ADVANCED
FUNCTIONAL
MATERIALS
www.afm-journal.de
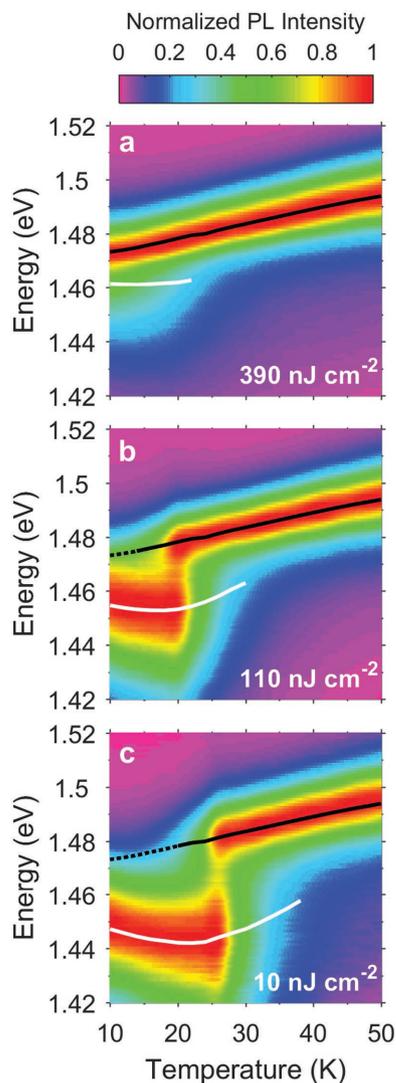
Figure 2. Temperature dependence of PL at different excitation fluences. Color plots of the normalized time-integrated PL spectra of FAPbI$_3$ at temperatures between 10 and 50 K, under excitation fluences of a) 390, b) 110, and c) 10 nJ cm^{-2}. The spectra were fitted with two Gaussian peaks, whose central energies are indicated by the solid black and white lines. The position of the higher energy peak at the lower fluences is inferred from the highest fluence data and plotted as dotted black lines. PL spectra at selected temperatures from these color plots are presented in Figure S2 (Supporting Information).

the sub-bandgap states may be best described by an exponential distribution for hybrid lead iodide perovskites.

2.2. Temperature Dependence of PL and Relative Stokes Shift

To establish the energy landscape of the trap distribution, we investigated the temperature dependence of the time-integrated PL spectra of FAPbI$_3$ for a range of excitation fluences (**Figure 2**). At higher temperatures, the PL spectra display a single dominant peak (black line, Figure 2) whose energy is independent of excitation fluence. This peak shifts monotonically upward in energy from about 1.475 eV at 10 K to 1.495 eV

at 50 K in accordance with the intrinsic behavior of the bandgap energy, which is known to blueshift with increasing temperature in hybrid lead halide perovskites.[18b,32] This blueshift is the opposite of that expected for typical semiconductors such as Si, Ge, and GaAs,[33] and has been attributed to the stabilization of band-edge states during thermal expansion of the lattice.[9,32] Indeed, the same atypical trend has been observed in the bandgaps of lead chalcogenides.[34] The blueshift of the higher-energy peak with temperature and its absence of saturation behavior suggest that this emission arises from the recombination of charge-carrier pairs delocalized in the band states of the semiconductor. These charge pairs most likely exist as free excitons since the thermal energies for the data shown in Figure 2 are below the exciton binding energy (14 meV)[35] for the low-temperature phase of FAPbI$_3$.

A second, very apparent feature in the PL at very low temperatures is a broad, lower-energy peak (white line, Figure 2) which exhibits saturation behavior, appearing less intense and higher in emission energy as the excitation fluence is increased (see also Figure S3, Supporting Information). The appearance of low-energy PL emission peaks in hybrid lead halide perovskites has been ascribed in previous studies to charge-carrier recombination at localized states.[36] Remarkably, we find here that such trap-mediated emission exhibits an anomalous energy shift with increasing temperature: while the peak energy of the band-edge emission from hybrid lead halide perovskites (black line) blueshifts with increasing temperature,[9] that of the trap-related emission (white line) initially exhibits a clear redshift. With increasing temperature, this effect leads to a widening energy gap, or relative Stokes shift, of the trap-mediated emission with respect to the free-exciton emission, which begins to reverse again for temperatures above ≈25 K. The relative Stokes shift differs from the conventional Stokes shift in its use of the energy of the free-exciton emission rather than the absorption onset as the reference point for the redshift.[37] Nonetheless, the fluence independence of the free-exciton PL peak over the measured range of fluences (as shown in Figure 2), combined with the temperature independence of the exciton binding energy, ensure that changes in the energy of the free-exciton PL peak with temperature reflect those of the band edge. The observed trend in the relative Stokes shift is at odds with the expected behavior of PL from discrete trap states or a well-defined indirect energy gap situated just below the bandgap. In both cases, the fixed energetic offset of the trap or indirect transition from the direct band edge would be equal to the (temperature-independent) relative Stokes shift as well as the thermal energy k_BT at which the peak disappeared.

We propose instead that the initial anomalous redshift (increased relative Stokes shift) arises from the presence of an energetic distribution of trap levels in the hybrid perovskite. At zero temperature, charge carriers have no thermal energy to move between sites and are therefore distributed randomly across the density of traps. With increasing temperature, sufficient thermal energy becomes available to activate the charge carriers over shallow barriers, allowing them to relax to deeper localized states before they recombine[38] thus decreasing the PL energy and increasing the relative Stokes shift. With further increase in temperature, the rate of hopping between states and phonon population both increase, resulting in the charge

**ADVANCED
SCIENCE NEWS**
www.advancedsciencenews.com

**ADVANCED
FUNCTIONAL
MATERIALS**
www.afm-journal.de

carriers becoming thermalized across the trap density of states (DOS).[31,39] The charge carriers therefore occupy a broader distribution of states with a higher average energy as the temperature increases, resulting in a blueshift[31] (decreased relative Stokes shift) and broadening[18b] of the PL emission. Such phenomena have also been observed in inorganic semiconductors such as AlGaN, InGaN, and AlInGaN,[38] where they have similarly been attributed to the motion of charge carriers within a band tail.[31,38,39] Here, we reveal that hybrid perovskites exhibit very similar trap-mediated emission with anomalous Stokes shifts. Importantly, as we show below, a quantitative analysis of this behavior allows us to extract directly the characteristic energy of the trap DOS that gives rise to these effects.

To enable such quantitative analysis, we extract the relative Stokes shifts from the data in Figure 2. The free-exciton and band-tail PL peaks were fitted with Gaussian functions to determine the peak energies, which are indicated in Figure 2 by the black and white lines, respectively. The relative Stokes shift is given by the energy difference between the peaks (i.e., the energetic separation between the black and white lines). When the free-exciton peak was not visible at low temperatures and fluences, the aforementioned fluence independence of the peak allowed its position to be inferred from the spectra taken at the highest fluence. The extracted relative Stokes shift is plotted in **Figure 3**b as a function of temperature for three different excitation fluences. Under the lowest excitation fluence of 10 nJ cm^{-2} implemented in our study, the largest relative Stokes shift of ≈37 meV is reached at a temperature of 25 K.

This is a consequence of the low charge-carrier density, which allows a majority of photoexcited carriers to relax deep into the band tail before they recombine. As the excitation fluence is increased, the higher initial charge-carrier density results in the filling of trap states, and the band-tail emission originates predominantly from higher-energy states closer to the band edge.

2.3. Quantitative Models of Anomalous Relative Stokes Shift

We verify our interpretation of the anomalous relative Stokes shift by use of quantitative models, which allow us to unravel the characteristic energy scale of the trap distribution. Unlike trap states associated with energetically well-defined defects, such as vacancies, substitutions, or interstitials,[11d,e,40] the energy scales at which band-tail PL emission occurs are not determined by a single energetic offset from the band edge but rather the charge-carrier occupation within a broader density of trap states. We explore two different approaches that have in the past been successfully used to describe the mechanisms of charge-carrier relaxation within band tails.[41] These are, first, a multiple-trapping model in which energetic relaxation occurs by thermal excitation to a shallower state followed by subsequent recapture (see Figure 3a for a schematic) and, second, a hopping model in which charge-carriers tunnel directly between states (Figure 3c). The two mechanisms, respectively, represent the limits of low and high overlap between band-tail states,[41] and therefore to assess properly the validity of the
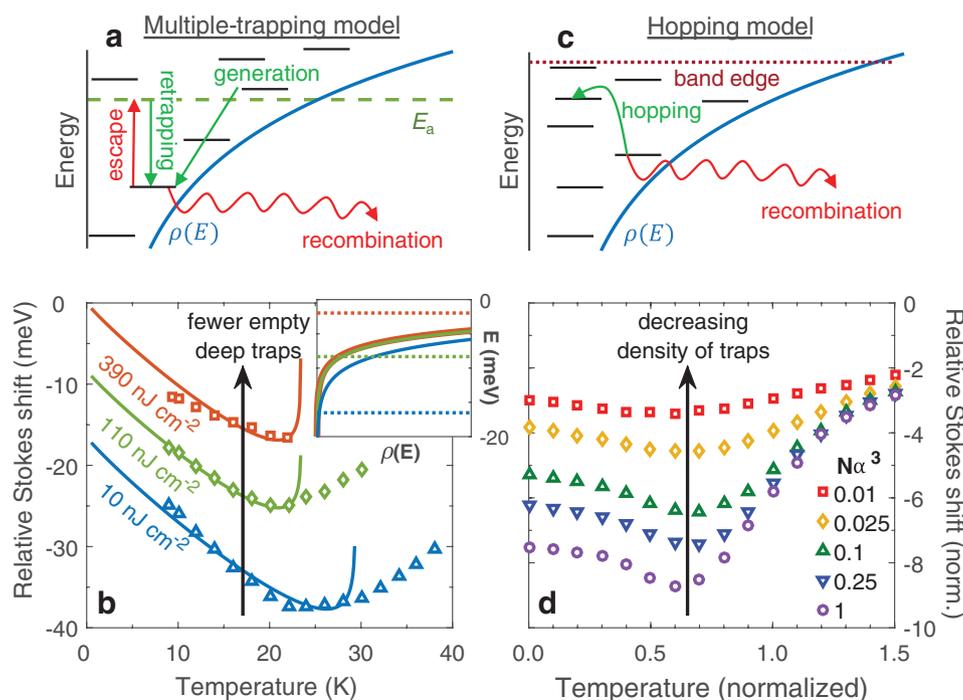
Figure 3. Models replicating the anomalous relative Stokes shift. a,c) Schematics of the multiple trapping (rate equation) and hopping (Monte Carlo) models of the anomalous relative Stokes shift respectively. b) The relative Stokes shift observed in FAPbI$_3$ is plotted, for excitation fluences of 390 (red), 110 (green), and 10 nJ cm^{-2} (blue). Fits to these data using the rate equation model are plotted as the matching colored lines. The inset shows the trap distributions corresponding to these fits, with the dotted lines showing the E_a values. The anomalous temperature dependence of the relative Stokes shifts can also be reproduced by Monte Carlo simulation of the hopping of charges in an exponential band tail, as shown in (d) for a range of trap state densities (represented by $N\alpha^3$). Here, the simulated relative Stokes shift and temperature are normalized against ε_0 and ε_0/k_B, respectively, where ε_0 is the inverse slope of the band tail. Simulated PL spectra at selected temperatures are presented in Figure S4 (Supporting Information).

ADVANCED
SCIENCE NEWS
www.advancedsciencenews.com

ADVANCED
FUNCTIONAL
MATERIALS
www.afm-journal.de

energy distribution extracted, we consider one model of each type: an elementary multiple-trapping model which produces an analytic function describing the relative Stokes shift, and a more sophisticated Monte Carlo model, which is a more physically accurate mechanism but requires more intense computational effort to model the data. In both cases, we consider the trap density of states to be approximated by exponential tails as the most realistic scenario for hybrid lead iodide perovskites. These models return a value of the characteristic energy ε_0 corresponding to the inverse slope of the trap density of states $\rho(\varepsilon) \propto e^{E/\varepsilon_0}$, which is defined for trap energies below the band edge at $E = 0$. Although 63% of the traps in the tail lie above ε_0, the tail naturally extends to energies much deeper into the bandgap, from where emission can still occur.

2.3.1. Multiple-Trapping Model

As a first approach, the multiple-trapping model[42] considers the mechanisms by which charge carriers may arrive at and leave states in the band tail to yield a rate equation describing the carrier dynamics (see schematic in Figure 3a). As detailed in the Supporting Information, this model assumes that charge carriers may only escape traps by thermal activation (with attempt-to-escape rate ν_e) to unoccupied states above energy E_a, from which they may be recaptured before eventually recombining radiatively (with lifetime τ_r). The nonmonotonic temperature dependence of the relative Stokes shift results from the upward redistribution of charge carriers within the band tail by thermal escape coming to dominate over the downward retrapping rate at higher temperatures. We here modify previously developed models for Gaussian band tails[42] to instead assume an exponential band tail, as described in the Supporting Information. The resulting peak PL energy associated with band-tail emission under pulsed excitation is then derived to be

$$E_{peak} = E_a + k_B T \ln \left[\frac{1}{\nu_e \tau_r} \frac{k_B T}{(\varepsilon_0 - k_B T)} \right] \tag{1}$$

for $\varepsilon_0 \leq k_B T$. In Figure 3b, Equation (1) is fitted to the relative Stokes shifts derived from Figure 2, with fitting parameters presented in the Supporting Information. As shown in the inset to Figure 3b, the lower charge-carrier concentration at lower fluence results in more traps deep in the band tail being left empty, corresponding to a deeper effective band-tail energy scale ε_0 and deeper energy E_a up to which state-filling occurs. The value of $\varepsilon_0 = 2.5$ meV under the lowest excitation fluence provides the best estimate of the characteristic energy scale of the band tail, though as can be seen from the inset to Figure 3b, the occupied states below the dotted line are in fact located far deeper. Indeed, it is not unusual for the deepest states in a band tail to exert a disproportionate influence on charge-carrier behavior,[43] since the tail theoretically descends indefinitely, allowing for broad PL emission from deep states even in a "shallow" tail. However, as expressed in Equation (1), ε_0 quantifies the thermal energy above which escape from the band-tail states becomes dramatically easier, such that charge carriers spend most of their time as free excitons and the trap emission fades.[44] Thus, a multiple-trapping model of charge-carrier recombination

within a band tail is able to rationalize the disparity between the energy scales of the maximum relative Stokes shift we observe at lowest fluences (≈40 meV) and the disappearance of the band-tail PL peak at temperatures corresponding to thermal energies $k_B T \approx 3$ meV. Such a shallow band tail is also consistent with the fading of clear power-law decay dynamics and trap-related emission peaks at an increased temperature of 100 K (Figure S5, Supporting Information), when charge carriers are thermally elevated to the upper levels of the DOS.

2.3.2. Hopping Model

As a second approach we model the anomalous relative Stokes shift as part of a charge hopping mechanism, using a more sophisticated Monte Carlo simulation to follow the relaxation of individual charge carriers within the band tail.[31] The details of the algorithm are given in the Supporting Information and a schematic diagram shown in Figure 3c. In outline, the charge carriers are introduced independently to a volume of localized states with randomly distributed positions and energies distributed according to the exponential band-tail DOS. When occupying a site i, a charge carrier can either recombine radiatively with lifetime τ_r, or tunnel to an empty site j according to the Miller–Abrahams rate[45]

$$\nu_{ij} = \nu_e \exp \left(-\frac{2r_{ij}}{\alpha} - \frac{E_j - E_i + |E_j - E_i|}{2k_B T} \right) \tag{2}$$

where ν_e is the attempt-to-escape frequency, α is the decay length of the localized exciton center-of-mass wavefunction, E_i and E_j are the energies of sites i and j, respectively, and r_{ij} is the distance between the sites. By generating random numbers, the stochastic behavior of each exciton is simulated, hopping between sites until it eventually undergoes radiative recombination. A histogram of the energies of the sites at which the excitons recombined produces the band-tail PL spectrum.

Simulations of the temperature dependence of the relative Stokes shift are shown in Figure 3d, for an exponential band tail, again of the form e^{E/ε_0}. The relative Stokes shift and temperature are both normalized, against ε_0 and ε_0/k_B, respectively. Each data series represents simulations for different values of the dimensionless parameter $N\alpha^3$, which quantifies the fraction of the volume per trap site that is occupied by the exciton wavefunction. The simulations reproduce the nonmonotonic temperature dependence of the relative Stokes shift observed in Figure 2. Decreasing $N\alpha^3$ represents a reduction in the concentration of localized states, corresponding to the lower availability of unoccupied sites for charge carriers to hop when the excitation fluence is higher. Indeed, the experimentally observed reduction in magnitude of the anomalous relative Stokes shift with increasing fluence is also observed at lower $N\alpha^3$. Notably, the maximum simulated relative Stokes shift occurs at ≈0.6 ε_0/k_B, independently of the choice of $N\alpha^3$ or other parameters.[37] Since our maximum experimental relative Stokes shift occurs at between 20 and 25 K, this allows the band-tail depth to be estimated from the Monte Carlo model as $\varepsilon_0 \approx 3$ meV, in excellent agreement with the rate equation model.

**ADVANCED
SCIENCE NEWS**

www.advancedsciencenews.com

**ADVANCED
FUNCTIONAL
MATERIALS**

www.afm-journal.de

3. Conclusion

Our results provide strong evidence that there is an exponential band tail of states in FAPbI$_3$ with a characteristic energy of 3 meV, obtained for both models irrespective of their opposing limits of low and high overlap between band-tail states. Power-law PL decays and anomalous Stokes shift are both features which necessitate the presence of an energetic distribution of trap states rather than well-defined defect levels. Band tails arise from continuous energetic disorder, which is not entirely unexpected in hybrid perovskites whose bandgaps are known to vary between films fabricated under different conditions.[46] By drawing together previous findings, we propose that the origin of the band-tail states in FAPbI$_3$ may lie in the rotational freedom of the polar organic cation,[47] which has been identified as a source of structural disorder in MAPbI$_3$.[48] Though less polar, the FA cation is larger than the MA cation and so distorts the perovskite lattice more.[32] In the low-temperature orthorhombic phase[35] of these materials, the rotational motion of the cations is frozen out,[35,49] resulting in static disorder and a shallow, varying potential from the long-range correlated orientations of the otherwise randomly oriented cation dipoles.[50] The local band minima and maxima resulting from these electrostatic potential fluctuations are prime candidates for localized states which form band tails.[50a,51] Such a model can also account for the power-law decay of the PL, since oppositely charged carriers are spatially separated within localized states randomly distributed in space, and can therefore only recombine after tunneling.[51] The degree of the energetic disorder could therefore be potentially tuned by substitution for the FA cation. We also note that our analysis can rule out the dominance of alternative trapping mechanisms that would be associated with discrete energy levels, such as specific elemental vacancies, substitutions, or interstitials, or the presence of a specific (discrete) indirect energy gap situated energetically just below the direct gap.

Our study reveals analogies with other, more established materials for photovoltaic applications. Energetic band tails have been found to feature in several such semiconductors, including Si, GaAs, and CIGS (CuIn$_x$Ga$_{1-x}$Se$_2$).[15b] An analysis of the energetic distribution of tail states is important for assessing a material's potential for photovoltaic applications because relaxation of charge carriers into the tail states results in a loss of open-circuit voltage V_{oc} relative to the bandgap energy. In FAPbI$_3$ solar cells at room temperature, the open-circuit voltage deficit relative to the bandgap was found to be ≈540 meV, which is comparable to CIGS but a greater deficit than for GaAs.[15b] The energy scale of the band tail we observed in FAPbI$_3$ is comparable to the Urbach energies of ≈1.5 and 10 meV calculated for GaAs and crystalline Si, respectively, at cryogenic temperatures.[52] Given that the room-temperature Urbach energy (15 meV[15b,16a]) of MAPbI$_3$ is also in the same range as that observed for other common photovoltaic materials (GaAs, 7 meV;[53] crystalline Si, 11 meV;[15b] amorphous Si 40 meV;[54] CIGS, 20 meV[55]), it would appear that our estimate of ε_0 = 3 meV is relatively typical for an inorganic semiconductor at low temperature, where the lower thermal disorder (which scales with $k_B T$) results in shallower band tails.[15b]

The relative shallowness of the band tail may also be a contributing factor to the high charge-carrier mobility observed for FAPbI$_3$.[56] In addition, our findings can clarify the thermally stimulated current peak observed by Baumann et al. at 27 K (corresponding to 2.3 meV),[8] and they suggest that long-lived PL components observed at room temperature[23] may result from slow residual charge-carrier recombination deep within the band tail. The value of 3 meV we determine for the characteristic energy of FAPbI$_3$ is shallower than the typical value of 15 meV measured for the Urbach energy in thin films of MAPbI$_3$, which may partly be due to these Urbach measurements having been taken at room temperature. A direct comparison at low temperature is not however possible, due to the disorder related to the incomplete phase transition which MAPbI$_3$ undergoes near 160 K which results in the formation of additional trap states in the low-temperature orthorhombic phase.[9,11a,18b] These traps most likely constitute inclusions of the high-temperature tetragonal phase[36d,57] and do not appear in FAPbI$_3$.[18b] Additional emission peaks associated with such traps in MAPbI$_3$ appear at energies ranging from ≈85[9,11a,57] to ≈300 meV[58] below the free-exciton emission, resulting in strong inhomogeneous broadening[18b] and precluding the observation of emission from a band tail of comparable characteristic energy to that we have observed here for FAPbI$_3$. The lower intrinsic degree of material disorder in FAPbI$_3$ may also contribute to the shallowness of the band tail.[18b]

Our overall analysis reveals the band-tail PL emission from FAPbI$_3$ to be consistent with typical behavior for an inorganic semiconductor, described by a band-structure picture with a relatively modest degree of energetic disorder as reflected by spatial variation of the bandgap energy. The maximum value of the anomalous relative Stokes shift we observe for FAPbI$_3$ at low charge-carrier densities (≈40 meV) is similar to the values observed in other inorganic semiconductors such as AlInGaN (≈45 meV),[38] GaInNAs (≈55 meV),[59] and CdSe/ZnSe (≈20 meV),[60] and band-tail emission has also been observed in CIGS and CZTS.[61] Despite often being misidentified until represented on a log-log plot,[25] power-law luminescence decays have also been identified in a range of systems, including semiconductor quantum dots,[62] dye-sensitized nanoparticle films,[63] and semiconductors such as hydrogenated amorphous Si,[54a] p-type GaAs,[64] and GaP.[65] Our observations and numerical analysis therefore highlight the general applicability of the classic inorganic semiconductor picture to hybrid lead halide perovskites, despite their partly organic ingredients.

In summary, we established the energetic distribution of trap states in FAPbI$_3$, a high-quality hybrid perovskite that is the active ingredient in some of the highest performing perovskite photovoltaic cells. Our measurements of low-temperature PL over six decades of time after excitation allowed the observation of a power-law time decay in the PL intensity, and an additional emission peak which exhibits an anomalous temperature dependence. We demonstrated qualitatively and quantitatively that both effects are the direct consequence of charge-carrier recombination in a band tail of states. Through numerical modeling, we were able to identify the characteristic energy scale of the band tail, which we propose to arise from local variations in electrostatic potential caused by different orientations of the polar FA cations. These discoveries provide valuable insight

**ADVANCED
SCIENCE NEWS**

www.advancedsciencenews.com

**ADVANCED
FUNCTIONAL
MATERIALS**

www.afm-journal.de

into the influence of trap states on charge-carrier recombination in this highly promising photovoltaic material.

4. Experimental Section

Sample Preparation: All materials unless otherwise stated were purchased from Sigma-Aldrich and used as received. Formamidinium iodide (FAI) was purchased from Dyesol. Thin films were prepared on Z-cut quartz substrates. These were initially cleaned sequentially with acetone followed by propan-2-ol, then treated with oxygen plasma for 10 min.

$FAPbI_3$ perovskite films were deposited using an acid-addition method to produce smooth and uniform pinhole-free films.[66] FAI and PbI_2 were dissolved in anhydrous N,N-dimethylformamide (DMF) (1:1 molar ratio at 0.55 M). Immediately prior to film formation, hydroiodic acid (38 µL, 57% w/w) was added to $FAPbI_3$ precursor solution (1 mL, 0.55 M) to enhance the solubility of the precursors and allow smooth and uniform film formation. Films were then spin-coated from the precursor plus acid solution on warm (85 °C) oxygen plasma-cleaned substrates at 2000 rotations per minute (rpm) in a nitrogen-filled glovebox, and subsequently annealed in air at 170 °C for 10 min. This heat treatment ensured that films were in the black perovskite phase of $FAPbI_3$, rather than the yellow hexagonal nonperovskite phase. Films continued to appear black throughout the study and showed no signs of yellowing or a reduction in emission that would be expected upon degradation into the non-photoactive yellow phase.

PL Spectroscopy: The samples were photoexcited by a 398 nm picosecond pulsed diode laser (PicoHarp, LDH-D-C-405M). The resultant PL was collected and coupled into a grating spectrometer (Princeton Instruments, SP-2558), which directed the spectrally dispersed PL onto an iCCD (PI-MAX4, Princeton Instruments) or a photon-counting detector (PDM series from MPD), whose timing was controlled with a PicoHarp300 TCSPC event timer. The sample was mounted under vacuum ($P < 10^{-6}$ mbar) in a cold-finger liquid helium cryostat (Oxford Instruments, MicrostatHe). An associated temperature controller (Oxford Instruments, ITC503) monitored the temperature at two sensors mounted on the heat exchanger of the cryostat and the end of the sample holder, respectively; the reading from the latter was taken as the sample temperature.

For the temperature-dependent measurements, PL spectra were taken with the iCCD as the sample was heated in increments of 2 K between 10 and 50 K. A pulse repetition rate of 10 kHz was used for the 390 nJ cm^{-2} measurements, and 1 kHz for the 110 and 10 nJ cm^{-2} measurements. For the time-dependent measurements, TCSPC data from 1 to 100 ns after excitation were meshed with iCCD data from 3 ns to 1 ms after excitation. A repetition rate of 1 kHz and a fluence of 390 nJ cm^{-2} were used. For the power-dependence measurements, the laser was used in continuous wave mode, and attenuated with a combination of neutral density filters, resulting in excitation intensities from 260 W cm^{-2} to 10 µW cm^{-2}.

Monte Carlo Methods: The Monte Carlo simulations were carried out in MATLAB according to the algorithm described in ref. [31] and summarized in the Supporting Information.

Supporting Information

Supporting Information is available from the Wiley Online Library or from the author.

Acknowledgements

Conflict of Interest

The authors declare no conflict of interest.

Keywords

[1] a) M. Liu, M. Johnston, H. Snaith, *Nature* **2013**, *501*, 395; b) W. S. Yang, J. H. Noh, N. J. Jeon, Y. C. Kim, S. Ryu, J. Seo, S. I. Seok, *Science* **2015**, *348*, 1234.

[2] a) L. M. Herz, *Annu. Rev. Phys. Chem.* **2016**, *67*, 65; b) M. B. Johnston, L. M. Herz, *Acc. Chem. Res.* **2016**, *49*, 146; c) Y.-H. Kim, H. Cho, T.-W. Lee, *Proc. Natl. Acad. Sci. USA* **2016**, *113*, 11694.

[3] J. S. Manser, J. A. Christians, P. V. Kamat, *Chem. Rev.* **2016**, *116*, 12956.

[4] L. Meng, E.-P. Yao, Z. Hong, H. Chen, P. Sun, Z. Yang, G. Li, Y. Yang, *Adv. Mater.* **2017**, *29*, 1603826.

[5] R. L. Milot, G. E. Eperon, T. Green, H. J. Snaith, M. B. Johnston, L. M. Herz, *J. Phys. Chem. Lett.* **2016**, *7*, 4178.

[6] S. G. Motti, M. Gandini, A. J. Barker, J. M. Ball, A. R. S. Kandada, A. Petrozza, *ACS Energy Lett.* **2016**, *1*, 726.

[7] T. Leijtens, G. E. Eperon, A. J. Barker, G. Grancini, W. Zhang, J. M. Ball, A. R. S. Kandada, H. J. Snaith, A. Petrozza, *Energy Environ. Sci.* **2016**, *9*, 3472.

[8] A. Baumann, S. Väth, P. Rieder, M. C. Heiber, K. Tvingstedt, V. Dyakonov, *J. Phys. Chem. Lett.* **2015**, *6*, 2350.

[9] M. I. Dar, G. Jacopin, S. Meloni, A. Mattoni, N. Arora, A. Boziki, S. M. Zakeeruddin, U. Rothlisberger, M. Graetzel, *Sci. Adv.* **2016**, *2*, e1601156.

[10] W.-J. Yin, T. Shi, Y. Yan, *Appl. Phys. Lett.* **2014**, *104*, 063903.

[11] a) R. L. Milot, G. E. Eperon, H. J. Snaith, M. B. Johnston, L. M. Herz, *Adv. Funct. Mater.* **2015**, *25*, 6218; b) D. Shi, V. Adinolfi, R. Comin, M. Yuan, E. Alarousu, A. Buin, Y. Chen, S. Hoogland, A. Rothenberger, K. Katsiev, Y. Losovyj, X. Zhang, P. A. Dowben, O. F. Mohammed, E. H. Sargent, O. M. Bakr, *Science* **2015**, *347*, 519; c) A. R. S. Kandada, S. Neutzner, V. D'Innocenzo, F. Tassone, M. Gandini, Q. A. Akkerman, M. Prato, L. Manna, A. Petrozza, G. Lanzani, *J. Am. Chem. Soc.* **2016**, *138*, 13604; d) S. D. Stranks, V. M. Burlakov, T. Leijtens, J. M. Ball, A. Goriely, H. J. Snaith, *Phys. Rev. Appl.* **2014**, *2*, 034007; e) Y. Yamada, T. Yamada, A. Shimazaki, A. Wakamiya, Y. Kanemitsu, *J. Phys. Chem. Lett.* **2016**, *7*, 1972.

[12] a) H.-S. Duan, H. Zhou, Q. Chen, P. Sun, S. Luo, T.-B. Song, B. Bob, Y. Yang, *PCCP* **2014**, *17*, 112; b) J. Kim, S.-H. Lee, J. H. Lee, K.-H. Hong, *J. Phys. Chem. Lett.* **2014**, *5*, 1312.

[13] W. Zhang, G. E. Eperon, H. J. Snaith, *Nat. Energy* **2016**, *1*, 16048.

[14] D. W. DeQuilettes, W. Zhang, V. M. Burlakov, D. J. Graham, T. Leijtens, A. Osherov, H. J. Snaith, D. S. Ginger, S. D. Stranks, *Nat. Commun.* **2016**, *7*, 11683.

[15] a) H. He, Q. Yu, H. Li, J. Li, J. Si, Y. Jin, N. Wang, J. Wang, J. He, X. Wang, Y. Zhang, Z. Ye, *Nat. Commun.* **2016**, *7*, 10896; b) S. De Wolf, J. Holovsky, S.-J. Moon, P. Löper, B. Niesen, M. Ledinsky, F.-J. Haug, J.-H. Yum, C. Ballif, *J. Phys. Chem. Lett.* **2014**, *5*, 1035.

[16] a) A. Sadhanala, F. Deschler, T. H. Thomas, S. E. Dutton, K. C. Goedel, F. C. Hanusch, M. L. Lai, U. Steiner, T. Bein, P. Docampo, D. Cahen, R. H. Friend, *J. Phys. Chem. Lett.* **2014**,

**ADVANCED
SCIENCE NEWS**

www.advancedsciencenews.com

**ADVANCED
FUNCTIONAL
MATERIALS**

www.afm-journal.de

5, 2501; b) Y. Yamada, T. Nakamura, M. Endo, A. Wakamiya, Y. Kanemitsu, *Appl. Phys. Express* **2014**, *7*, 032302.

[17] V. Sa-Yakanit, N. R. Glyde, *Comments Condens. Matter Phys.* **1987**, *13*, 35.

[18] a) J. Endres, D. A. Egger, M. Kulbak, R. A. Kerner, L. Zhao, S. H. Silver, G. Hodes, B. P. Rand, D. Cahen, L. Kronik, A. Kahn, *J. Phys. Chem. Lett.* **2016**, *7*, 2722; b) A. D. Wright, C. Verdi, R. L. Milot, G. E. Eperon, M. A. Pérez-Osorio, H. J. Snaith, F. Giustino, M. B. Johnston, L. M. Herz, *Nat. Commun.* **2016**, *7*, 11755.

[19] a) A. Buin, R. Comin, J. Xu, A. H. Ip, E. H. Sargent, *Chem. Mater.* **2015**, *27*, 4405; b) X. Fang, K. Zhang, Y. Li, L. Yao, Y. Zhang, Y. Wang, W. Zhai, L. Tao, H. Du, G. Ran, *Appl. Phys. Lett.* **2016**, *108*, 071109.

[20] D. Bi, W. Tress, M. I. Dar, P. Gao, J. Luo, C. Renevier, K. Schenk, A. Abate, F. Giordano, J.-P. C. Baena, J.-D. Decoppet, S. M. Zakeeruddin, M. K. Nazeeruddin, M. Grätzel, A. Hagfeldt, *Sci. Adv.* **2016**, *2*, e1501170.

[21] a) N. K. Noel, A. Abate, S. D. Stranks, E. Parrott, V. Burlakov, A. Goriely, H. J. Snaith, *ACS Nano* **2014**, *8*, 9815; b) G. Xing, N. Mathews, S. Sun, S. S. Lim, Y. M. Lam, M. Grätzel, S. Mhaisalkar, T. C. Sum, *Science* **2013**, *342*, 344.

[22] P. W. Liang, C. Y. Liao, C. C. Chueh, F. Zuo, S. T. Williams, X. K. Xin, J. Lin, A. K. Y. Jen, *Adv. Mater.* **2014**, *26*, 3748.

[23] Q. Han, S.-H. Bae, P. Sun, Y.-T. Hsieh, Y. M. Yang, Y. S. Rim, H. Zhao, Q. Chen, W. Shi, G. Li, Y. Yang, *Adv. Mater.* **2016**, *28*, 2253.

[24] a) D. W. DeQuilettes, S. M. Vorpahl, S. D. Stranks, H. Nagaoka, G. E. Eperon, M. E. Ziffer, H. J. Snaith, D. S. Ginger, *Science* **2015**, *348*, 683; b) X. Li, D. Bi, C. Yi, J.-D. Decoppet, J. Luo, S. M. Zakeeruddin, A. Hagfeldt, M. Gratzel, *Science* **2016**, *353*, 58.

[25] A. K. Jonscher, A. de Polignac, *J. Phys. C: Solid State Phys.* **1984**, *17*, 6493.

[26] M. Kuno, D. P. Fromm, H. F. Hamann, A. Gallagher, D. J. Nesbitt, *J. Chem. Phys.* **2000**, *112*, 3117.

[27] D. J. Huntley, *J. Phys.: Condens. Matter* **2006**, *18*, 1359.

[28] J. T. Randall, M. H. F. Wilkins, *Proc. R. Soc. London, Ser. A* **1945**, *184*, 390.

[29] D. J. Dunstan, F. Boulitrop, *Phys. Rev. B* **1984**, *30*, 5945.

[30] a) P. G. Eliseev, M. Osinski, J. Lee, T. Sugahara, S. Sakai, *J. Electron. Mater.* **2000**, *29*, 332; b) T. Tiedje, A. Rose, *Solid State Commun.* **1981**, *37*, 49.

[31] S. Baranovskii, R. Eichmann, P. Thomas, *Phys. Rev. B* **1998**, *58*, 13081.

[32] J. M. Frost, K. T. Butler, F. Brivio, C. H. Hendon, M. van Schilfgaarde, A. Walsh, *Nano Lett.* **2014**, *14*, 2584.

[33] Y. P. Varshni, *Physica* **1967**, *34*, 149.

[34] A. Svane, N. E. Christensen, M. Cardona, A. N. Chantis, M. Van Schilfgaarde, T. Kotani, *Phys. Rev. B* **2010**, *81*, 1.

[35] K. Galkowski, A. Mitioglu, A. Miyata, P. Plochocka, O. Portugall, G. E. Eperon, J. T.-W. Wang, T. Stergiopoulos, S. D. Stranks, H. J. Snaith, R. J. Nicholas, *Energy Environ. Sci.* **2016**, *9*, 962.

[36] a) H.-H. Fang, R. Raissa, M. Abdu-Aguye, S. Adjokatse, G. R. Blake, J. Even, M. A. Loi, *Adv. Funct. Mater.* **2015**, *25*, 2378; b) H.-H. Fang, F. Wang, S. Adjokatse, N. Zhao, J. Even, M. A. Loi, *Light: Sci. Appl.* **2016**, *5*, e16056; c) W. Kong, Z. Ye, Z. Qi, B. Zhang, M. Wang, A. Rahimi-Iman, H. Wu, E. Lifshitz, H. Yassen, L. Bykov, I. Dag, *PCCP* **2015**, *17*, 16405; d) F. Panzer, S. Baderschneider, T. P. Gujar, T. Unger, S. Bagnich, M. Jakoby, H. Bässler, S. Hüttner, J. Köhler, R. Moos, M. Thelakkat, R. Hildner, A. Köhler, *Adv. Opt. Mater.* **2016**, *4*, 917; e) J. Tilchin, D. N. Dirin, G. I. Maikov, A. Sashchiuk, M. V. Kovalenko, E. Lifshitz, *ACS Nano* **2016**, *10*, 6363; f) C. Wehrenfennig, M. Liu, H. J. Snaith, M. B. Johnston, L. M. Herz, *Energy Environ. Sci.* **2014**, *7*, 2269; g) G. Xing,

N. Mathews, S. S. Lim, N. Yantara, X. Liu, D. Sabba, M. Grätzel, S. Mhaisalkar, T. C. Sum, *Nat. Mater.* **2014**, *13*, 476.

[37] O. Rubel, M. Galluppi, S. D. Baranovskii, K. Volz, L. Geelhaar, H. Riechert, P. Thomas, W. Stolz, *J. Appl. Phys.* **2005**, *98*, 063518.

[38] K. Kazlauskas, G. Tamulaitis, A. Žukauskas, M. A. Khan, J. W. Yang, J. Zhang, G. Simin, M. S. Shur, R. Gaska, *Appl. Phys. Lett.* **2003**, *83*, 3722.

[39] I. Friel, C. Thomidis, T. D. Moustakas, *Appl. Phys. Lett.* **2004**, *85*, 3068.

[40] W. J. Yin, T. Shi, Y. Yan, *Adv. Mater.* **2014**, *26*, 4653.

[41] D. Monroe, *Phys. Rev. Lett.* **1985**, *54*, 146.

[42] Q. Li, S. J. Xu, W. C. Cheng, M. H. Xie, S. Y. Tong, C. M. Che, H. Yang, *Appl. Phys. Lett.* **2001**, *79*, 1810.

[43] S. D. Baranovskii, *Phys. Status Solidi B* **2014**, *251*, 487.

[44] R. Könenkamp, *Photoelectric Properties and Applications of Low-Mobility Semiconductors*, Springer, Berlin **2000**.

[45] A. Miller, E. Abrahams, *Phys. Rev.* **1960**, *120*, 745.

[46] a) M. De Bastiani, V. D'Innocenzo, S. D. Stranks, H. J. Snaith, A. Petrozza, *APL Mater.* **2014**, *2*, 081509; b) G. Grancini, S. Marras, M. Prato, C. Giannini, C. Quarti, F. De Angelis, M. De Bastiani, G. E. Eperon, H. J. Snaith, L. Manna, A. Petrozza, *J. Phys. Chem. Lett.* **2014**, *5*, 3836.

[47] R. E. Wasylishen, O. Knop, J. B. Macdonald, *Solid State Commun.* **1985**, *56*, 581.

[48] E. Juarez-Perez, R. Sanchez, *J. Phys. Chem. Lett.* **2014**, *5*, 2390.

[49] T. Baikie, Y. Fang, J. M. Kadro, M. Schreyer, F. Wei, S. G. Mhaisalkar, M. Gratzel, T. J. White, M. Graetzel, T. J. White, M. Gratzel, T. J. White, *J. Mater. Chem. A* **2013**, *1*, 5628.

[50] a) J. Ma, L.-W. Wang, *Nano Lett.* **2015**, *15*, 248; b) S. A. March, D. B. Riley, C. Clegg, D. Webber, X. Liu, M. Dobrowolska, J. K. Furdyna, I. G. Hill, K. C. Hall, *arXiv preprint arXiv:1602.05186*, **2016**.

[51] T. Gokmen, O. Gunawan, T. K. Todorov, D. B. Mitzi, *Appl. Phys. Lett.* **2013**, *103*, 103506.

[52] C. W. Greeff, H. R. Glyde, *Phys. Rev. B* **1995**, *51*, 1778.

[53] O. D. Miller, E. Yablonovitch, S. R. Kurtz, *IEEE J, Photovoltaics* **2012**, *2*, 303.

[54] a) R. A. Street, *Adv. Phys.* **1981**, *30*, 593; b) T. Tiedje, *Appl. Phys. Lett.* **1982**, *40*, 627.

[55] J. T. Heath, J. D. Cohen, W. N. Shafarman, D. X. Liao, A. A. Rockett, *Appl. Phys. Lett.* **2002**, *80*, 4540.

[56] W. Rehman, R. L. Milot, G. E. Eperon, C. Wehrenfennig, J. L. Boland, H. J. Snaith, M. B. Johnston, L. M. Herz, *Adv. Mater.* **2015**, *27*, 7938.

[57] C. Wehrenfennig, M. Liu, H. J. Snaith, M. B. Johnston, L. M. Herz, *APL Mater.* **2014**, *2*, 081513.

[58] L. Q. Phuong, Y. Yamada, M. Nagai, N. Maruyama, A. Wakamiya, Y. Kanemitsu, *J. Phys. Chem. Lett.* **2016**, *7*, 2316.

[59] H. Grüning, K. Kohary, S. D. Baranovskii, O. Rubel, P. J. Klar, A. Ramakrishnan, G. Ebbinghaus, P. Thomas, W. Heimbrodt, W. Stolz, W. W. Rühle, *Phys. Status Solidi C* **2004**, *1*, 109.

[60] B. Dal Don, K. Kohary, E. Tsitsischvili, R. Eichmann, S. D. Baranovskii, P. Thomas, H. Kalt, *Phys. Status Solidi C* **2003**, *0*, 1509.

[61] M. J. Romero, H. Du, G. Teeter, Y. Yan, M. M. Al-Jassim, *Phys. Rev. B* **2011**, *84*, 1.

[62] M. Menšik, K. Kral, *Microelectron. Eng.* **2013**, *111*, 170.

[63] I. J. McNeil, D. L. Ashford, H. Luo, C. J. Fecko, *J. Phys. Chem. C* **2012**, *116*, 15888.

[64] R. Dingle, *Phys. Rev.* **1969**, *184*, 788.

[65] D. G. Thomas, J. J. Hopfield, W. M. Augustyniak, *Phys. Rev.* **1965**, *140*, 202.

[66] G. E. Eperon, S. D. Stranks, C. Menelaou, M. B. Johnston, L. M. Herz, H. J. Snaith, *Energy Environ. Sci.* **2014**, *7*, 982.

1700860 (8 of 8)